Hindawi Publishing Corporation
Journal of Nanomaterials
Volume 2014, Article ID 192797, 10 pages
http://dx.doi.org/10.1155/2014/192797

Research Article

Tuning the Morphological Structure and Photocatalytic Activity of Nitrogen-Doped $(BiO)_2CO_3$ by the Hydrothermal Temperature

Chongjun Wang,[1] Zaiwang Zhao,[1] Bin Luo,[1] Min Fu,[1,2] and Fan Dong[1,2]

[1] *Chongqing Key Laboratory of Catalysis and Functional Organic Molecules, College of Environmental and Biological Engineering, Chongqing Technology and Business University, Chongqing 400067, China*
[2] *Chongqing Key Laboratory for Urban Atmospheric Environment Integrated Observation & Pollution Prevention and Control, Environmental Monitoring Center of Chongqing, Chongqing 401147, China*

Correspondence should be addressed to Min Fu; fumin1022@126.com

Received 21 November 2013; Accepted 2 January 2014; Published 13 February 2014

Academic Editor: Haiqiang Wang

Various nitrogen-doped hierarchical $(BiO)_2CO_3$ nanosheets architectures were synthesized by a facile one-step template-free hydrothermal method through controlling the hydrothermal temperature (HT). The as-synthesized samples were characterized by XRD, SEM, FT-IR, XPS, and UV-vis DRS. The photocatalytic activity of the samples was evaluated towards degradation of NO at ppb level in air under visible light (VIL). It was found that HT acted as a crucial factor in determining the morphology of the samples. The rosa chinensis-like, red camellia-like, and lamina-like of nitrogen-doped $(BiO)_2CO_3$ (N-BOC) micro-/nanostructures can be selectively fabricated under hydrothermal temperatures of 150, 180, and 210°C. The thickness of the nanosheets was in direct proportion to the increasing HT. Nitrogen-doping can extend the light absorption spectra of $(BiO)_3CO_3$ to visible light region and enhance the VIL photocatalytic activity. Especially, the red camellia-like N-BOC-180 exhibited the highest photocatalytic performance, superior to the well-known VIL-driven photocatalyst C-doped TiO_2 and N-doped TiO_2. The high photocatalytic performance of N-BOC was attributed to the synergetic effects of enhanced visible light absorption, multiple light-reflections between the nanosheets, and accelerated transfer of reactants and product. This research could provide new insights to the development of excellent photocatalyst with efficient performance for pollution control.

1. Introduction

Over the past decades, photocatalysis technology has attracted tremendous attention due to its great potential in solving energy and environmental problems [1]. Generally, photocatalysts were semiconductor materials, among which, TiO_2 bears tremendous hope in helping ease the energy crisis and environment pollution [2, 3]. However, the shortage of demanding UV light in the solar energy severely impedes the scale-up application of TiO_2 [4–6]. Therefore, it is imperative to explore novel photocatalyst with enhanced visible light (VIL) absorption. Generally, two strategies were applied to develop visible-light-driven photocatalysts. One is chemical modification on the UV-driven photocatalysts, such as TiO_2, willing to narrow the band gap [7]. The other is to fabricate new types of semiconductor with narrow band gap working directly under visible light [8].

Bismuth compounds, such as $BiVO_4$, Bi_2MoO_6, Bi_2WO_6, and BiOX (X = Cl, Br, I), have received considerable attention due to their high visible light photocatalytic activity [9–13]. A typical "Sillén" phase was reported by Grice's group [14]. $(BiO)_2CO_3$ belongs to the Aurivillius-related oxide family and owns an intergrowth of $Bi_2O_2^{2+}$ layers and CO_3^{2-} layers, with the plane of the CO_3^{2-} group orthogonal to the plane of the $Bi_2O_2^{2+}$ layer. Although bismuth subcarbonate $(BiO)_2CO_3$ was first used for medical and healthcare application, it also joined the photocatalyst family because of its semiconductor properties. For example, Zheng et al. reported the photocatalytic activity of the $(BiO)_2CO_3$, and discovered that samples with {001} plane exposed demonstrate the best

photocatalytic activities [15]. Liu et al. obtained $(BiO)_2CO_3$ nanoflowers at relatively low temperature of 60°C, exhibiting high photocatalytic efficiency towards the degradation of wastewater dyes under UV-vis light irradiation [16]. Chen et al. synthesized $(BiO)_2CO_3$ with different morphology which exhibited enhanced antibacterial properties [17]. Zhou et al. prepared nanostructured $Bi_2O_2CO_3$ by an environmentally friendly method and applied the material in humidity sensing [18]. Besides, photocatalysts with microsphere structure demonstrated fascinating photocatalytic activity. For example, Zhao et al. fabricated hierarchical rose-like $(BiO)_2CO_3$ microspheres with superior photocatalytic property under sunlight [19]. Dong et al. prepared rose-like monodisperse bismuth subcarbonate hollow microspheres through one-pot template-free method, accompanied with high NO degradation under modulated solar light irradiation [20]. Also, Madhusudan et al. fabricated hierarchical $(BiO)_2CO_3$ microstructures with decent photocatalytic activities in degradation of organic dyes under visible light [21]. Recently, Dong et al. have prepared uniform $(BiO)_2CO_3$ hierarchical hollow microspheres with outstanding photocatalytic activities under both UV and visible light [22]. The formation of hollow hierarchical inorganic micro- and nanostructures can be ascribed to the synergetic effects of the well-known physical phenomena, such as, Ostwald ripening [23], Kirkendall-effect, and oriented attachment [24, 25]. Furthermore, the enhanced photocatalytic activity of flower-like microsphere nanostructures can be ascribed to the strengthened light absorption due to the multiple reflections between the nanosheets and hierarchical microstructures which is beneficial to improve light-harvesting efficiency [26].

Hierarchical hollow structured materials were usually synthesized based on templating approaches, which contain hard templates and soft templates [27–35]. Template synthesis usually suffers from tedious processes, including template modification, precursor attachment, and core removal [36, 37], which may lead to a cumbersome process and reluctant overexpenditure, limiting the potential applications. Hence, development of facile template-free methods for obtaining inorganic hierarchical architectures is highly desirable. Facile template-free methods could obviously simplify the fabrication process, cut down the production expenditure, and promote large-scale applications of hierarchical materials.

Following a breakthrough that Asahi et al. firstly discovered that nitrogen doping can promote the VIL photocatalytic activity of TiO_2 by reducing the band gap of TiO_2, various types of nonmetal-doped TiO_2 have been explored [38, 39]. Among them, N-doped TiO_2 is the most representative and has been on the focus of intensive investigation [39]. Although nitrogen doping is still under dispute, the concept of nitrogen doping has been successfully applied to narrow the band gap of various types of photocatalyst, such as Bi_3NbO_7, $SrTiO_3$, and $Sr_2Ta_2O_7$ [40–42]. Inspired by the convenient scale-up N-doping processes to gain favourable VIL activity, it is potentially feasible to apply this strategy to $(BiO)_2CO_3$ with large band gap, aiming to narrow the band gap of $(BiO)_2CO_3$. Recently, Dong et al. have synthesized N-doping of $(BiO)_2CO_3$ (N-BOC) hierarchical microspheres self-assembled with nanoplates using bismuth citrate and ammonia as precursors [43, 44]. It was found that the content of ammonia and the hydrothermal temperature imparted significant effects on the microstructure and activity of N-BOC [43, 44]. Though some advances have been made on the fabrication of N-BOC nanostructured materials, current knowledge about physical chemical properties and formation mechanisms on N-BOC architectures is still limited. It is necessary to explore and systematically unravel the influence factors that determine the potential growth pattern, physical chemical properties and, photocatalytic activity of the samples.

Herein, we implement a temperature-dependent research to explore the influence of hydrothermal temperature (HT) on morphology and photocatalytic activity of N-BOC micro-/nanostructures. We synthesized novel N-BOC materials via a template-free hydrothermal method based on aqueous solution of bismuth citrate and concentrated ammonia with HT changing from 150, 180 to 210°C, respectively. As a result, diverse morphology of N-BOC microstructures can be selectively fabricated upon different HT. Besides, HT plays a crucial role in determining the photocatalytic activity of N-BOC. Furthermore, it is worthy to note that N-BOC-180 exhibited enhanced photocatalytic activity compared with samples proceeded in 150°C and 210°C, exceeding that of other typical VIL photocatalysts C-doped TiO_2 and N-doped TiO_2.

2. Experimental

2.1. Fabrication of $(BiO)_2CO_3$ Nano-/Microstructures. All chemicals were analytical grade (sigma Aldrich) and were used without further purification. In a typical fabrication, appropriate amounts of bismuth citrate (1.6 g) were dissolved in concentrated ammonia solution (28 wt%) of 7.6 mL. The acquired transparent solution was stirred for 5 min. Distilled water was added to the obtained solution to make the total volume of 75 mL. The mixture was transferred to an autoclave Teflon vessel of 100 mL and stirred for 30 min. The aqueous precursor suspension was then hydrothermally treated under different HT for 24 h. After the hydrothermal reaction, the solid product was collected by filtration, washed with distilled water and ethanol four times, and dried at 60°C to get the final N-doping of $(BiO)_2CO_3$ without further disposal. Depending on the HT (150, 180, and 210°C), N-doped $(BiO)_2CO_3$ with different morphologies can be fabricated and labeled as N-BOC-150, N-BOC-180, and N-BOC-210, respectively. Comparing to the photocatalytic activity, N-doped TiO_2 and C-doped TiO_2 were used as reference samples [45, 46].

2.2. Characterization. The crystal phase was analyzed by X-ray diffraction with Cu Kα radiation (XRD: model D/max RA, Japan). The morphology was characterized by scanning electron microscope (SEM, JEOL model JSM-6490, Japan). The UV-vis diffuse reflection spectra were obtained using a Scan UV-vis spectrophotometer (UV-vis DRS: UV-2450, shimadzu, Japan) equipped with an integrating sphere assembly, using $BaSO_4$ as reflectance sample. FT-IR spectra were recorded on a Nicolet Nexus spectrometer on samples

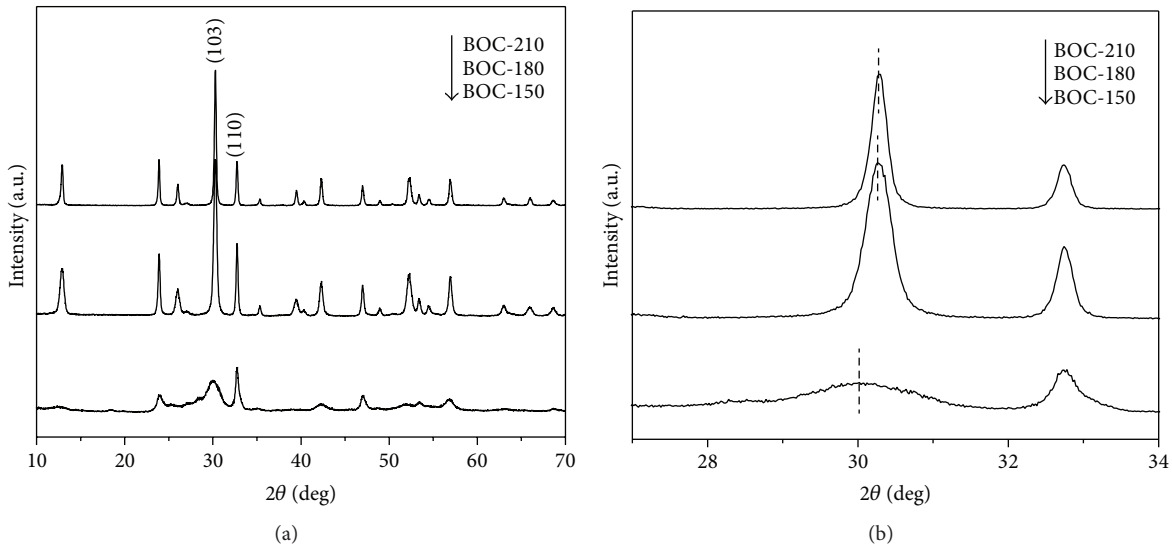

Figure 1: XRD patterns of N-BOC-150, N-BOC-180, and N-BOC-210 samples (a) and enlarged view of (103) and (110) diffraction region (b).

embedded in KBr pellets. X-ray photoelectron spectroscopy with Al KαX-rays ($h\nu$ = 1486.6 eV) radiation operated at 150 W (XPS: Thermo ESCALAB 250, USA) was used to investigate the surface properties. Nitrogen adsorption-desorption was conducted on a nitrogen adsorption apparatus (ASAP 2020, USA) to determine the specific surface areas. All the samples were degassed at 150°C prior to measurements.

2.3. Evaluation of Photocatalytic Activity. The photocatalytic activity was investigated by removal of NO at ppb levels in a continuous flow reactor at ambient temperature. The volume of the rectangular reactor, which was made of polymethyl methacrylate plastics and covered with Saint-Glass, was 4.5 L (30 cm × 15 cm × 10 cm). A 100 W commercial tungsten halogen lamp (General Electric) was vertically placed outside the reactor above the reactor. Four minifans were used to cool the flow system. Adequate distance was also kept from the slamp to the reactor for the same purpose to keep the temperature at a constant level. For the visible light photocatalytic activity test experiment, UV cutoff filter (420 nm) was adopted to remove UV light in the light beam. For each photocatalytic activity test, two sample dishes (with a diameter of 12.0 cm) containing 0.1 g of photocatalyst powder were placed in the center of reactor. The photocatalyst samples were prepared by coating aqueous suspension of the samples onto the glass dishes. The coated dish was pretreated at 70°C to remove water in the suspension and then cooled to room temperature before photocatalytic test. The NO gas was acquired from a compressed gas cylinder at a concentration of 100 ppm of NO (N_2 balance, BOC gas) with traceable National Institute of Standards and Technology (NIST) standard. The initial concentration of NO was diluted to about 630 ppb by the air stream supplied by a zero air generator (Thermo Environmental Inc., model 111). The desired relative humidity (RH) level of the NO flow was controlled at 70% by passing the zero air streams through a humidification chamber. The gas streams were premixed completely by a gas blender, and the flow rate was controlled at 2.4 L min^{-1} by a mass flow controller. After the adsorption-desorption equilibrium was achieved, the lamp was turned on. The concentration of NO was continuously measured by a chemiluminescence NO analyzer (Thermo Environmental Instruments Inc., model 42c), which monitors NO, NO_2, and NOx (NOx represents NO + NO_2) with a sampling rate of 0.7 L min^{-1}. The removal ratio (η) of NO was calculated as

$$\eta\,(\%) = \left(1 - \frac{C}{C_0}\right) \times 100\%, \tag{1}$$

where C and C_0 are concentrations of NO in the outlet steam and the feeding stream, respectively.

3. Results and Discussion

3.1. Phase Structure. XRD was used to investigate the phase structure of the obtained powders. Figure 1(a) shows the XRD patterns of all as-prepared samples. All the diffraction peaks can be indexed to the tetragonal phase of $(BiO)_2CO_3$ compared with standard PDF card (JCPDS-ICDD Card No. 25-1464). The growth tendency of (110) peak always rises up gradually as HT increases from 150, 180 to 210°C, compared with that of (103) peek initially increases as HT increases from 150°C to 180°C but subsequently decreases as HT increases from 180°C to 210°C. The above results also suggest that HT has a significant effect on the crystallinity of all samples and the relative higher temperature benefits the preferred crystal growth along the (110) planes. Further observation in the enlarged view of XRD in Figure 1(b) indicates that the dominant (103) diffraction peak exhibits higher diffraction angles with HT increasing from 150, 180 to 210°C. These results implied that the distance between crystal planes slightly decreased under higher HT, demonstrating that the crystal structure tends to be more stable.

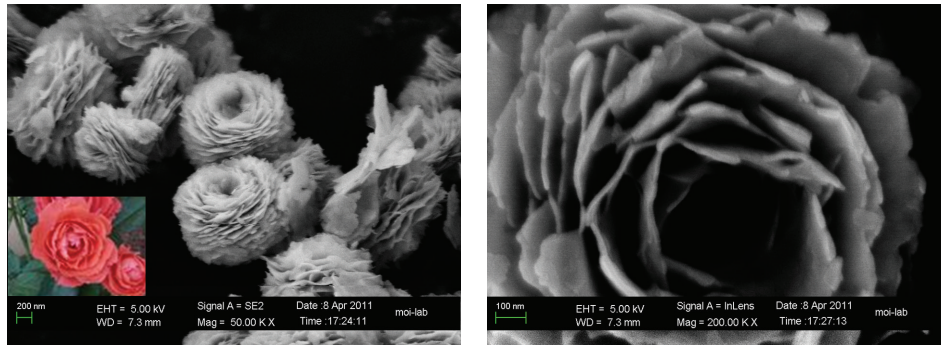

(a) (b)

Figure 2: SEM images for N-BOC-150 ((a), (b)).

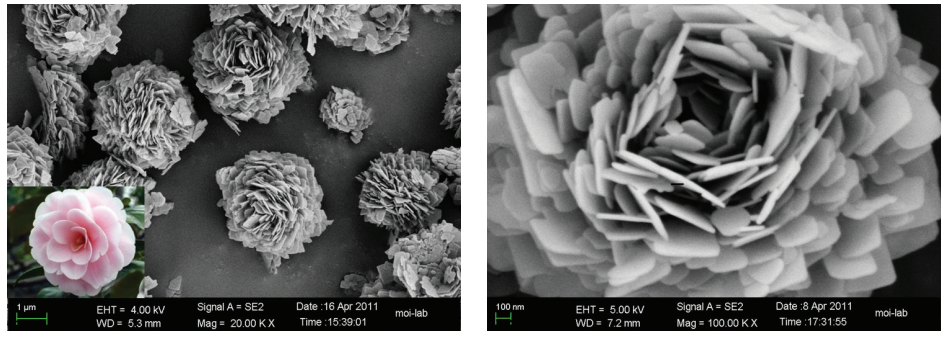

(a) (b)

Figure 3: SEM images for N-BOC-180 ((a), (b)).

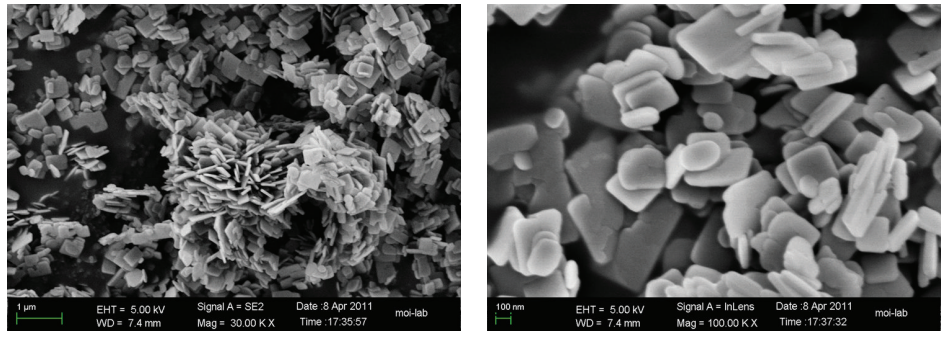

(a) (b)

Figure 4: SEM images for N-BOC-210 ((a), (b)).

3.2. Morphological Evolution. Figures 2, 3, and 4 show typical SEM images of the as-prepared products, where large quantity of uniform $(BiO)_2CO_3$ hierarchical microflowers composed of 2D nanosheets can be observed. No other morphologies could be found, which demonstrates the high yield of the hierarchical microstructures. The SEM images with higher magnification (Figures 2(b), 3(b), and 4(b)) give more detailed structural information of the microstructures, which are closely related to the photocatalytic activity.

For N-BOC-150 sample, a large number of rosa chinensis-like hierarchical microspheres, with a concavity in the center, were shown in the typical SEM images in Figure 2(a). The higher magnification SEM image (Figure 2(b)) reveals that these monodisperse rosa chinensis-like microspheres have average diameter of about 1.2 μm with a concavity in the center of about 0.5 μm. The special nanostructures are self-assembled by many thin nanosheets in a hierarchical form. The nanosheets are arranged at progressively increasing angles to the radial axis and highly directed to form arrays in

Table 1: Morphology, average microsphere diameter, average concavity diameter, and nanosheets thickness of N-BOC-150, N-BOC-180, and N-BOC-210 samples.

Samples	Morphology	Average microsphere diameter (μm)	Average concavity diameter (μm)	Nanosheets thickness (nm)
N-BOC-150	Rosa chinensis-like	1.2	0.5	27
N-BOC-180	Red camellia-like	3.0	1.1	36
N-BOC-210	Lamina-like	—	—	47

a hierarchical fashion, which is advantageous for promoting the photocatalytic activity by enhancing the photo-energy harvesting and strengthening reactants transfer to the interior space.

For N-BOC-180 sample, the morphology of nitrogen-doped $(BiO)_2CO_3$ is transformed into large numbers of red camellia-like hierarchical microspheres (Figure 3(a)). The average diameter of the microspheres is increased to about 3.0 μm and the average diameter of the concavity is increased to about 1.1 μm (Figure 3(b)). The red camellia-like microspheres are also organized by hierarchically self-assembled nanosheets. When the HT increases from 150 to 180°C, the thickness of the nanosheets is increased from 27 to 36 nm (Table 1). According to above observations, the as-prepared nitrogen-doping of $(BiO)_2CO_3$ microstructures can be classified as hierarchical microflowers obtained through the oriented self-assembly of nanosheets. Although the nanosheets do not pack densely, the $(BiO)_2CO_3$ microflowers cannot collapse into dispersed nanosheets, even after long-time ultrasonication.

For N-BOC-210 sample, the microstructure of nitrogen-doped $(BiO)_2CO_3$ consists of large numbers of irregular aggregated lamina-like nanosheets (Figure 4(a)), which is obviously different from N-BOC-150 and N-BOC-180. The average thickness of the nanosheets is about 47 nm, which is further increased compared with that of others under HT of 150 and 180°C (Figure 4(b)). The SEM image with higher magnification (Figure 4(b)) shows that the obtained compound consists of plentiful different sizes of nanosheets with irregular shape.

The SEM images in Figure 2-4 imply that the HT plays a crucial role in forming various morphology of N-doped $(BiO)_2CO_3$ nano/microstructures. As HT increases, thickness of the nanoplates augments correspondingly. At low temperatures of 150 and 180°C, the nanosheets could self-assemble to construct hierarchical microspheres. Nevertheless, the nanosheets could not be self-assembled as the HT increases to 210°C, due to the accelerating hydrothermal reaction and the increasing thickness, forming randomly and irregularly arranged lamina-like nanoplates. The S_{BET} values of as-prepared N-BOC obtained at 150, 180, and 210°C were 22, 21, and 13 m^2/g, respectively, which is consistent with microstructures of the samples (Table 2). Dong has revealed the effect of hydrothermal temperature on the morphological structure of N-BOC from bismuth citrate (1.6 g) and concentrated ammonia solution (1.9 mL). However, the present investigation increased the content of concentrated ammonia solution to 7.8 mL and found that the hydrothermal temperature has different effects on the morphological structure. Especially when the temperature was increased to 210°C, the microspheres were destroyed (Figure 4(b)), which was different from the previous report [44].

Table 2: BET surface areas, reaction constants, and NO removal ratio of N-BOC-150, N-BOC-180, and N-BOC-210.

Samples	S_{BET} (m^2/g)	Reaction constants (k/min^{-1})	Removal ratio (%)
N-BOC-150	22	0.6570	24.7
N-BOC-180	21	1.2698	44.1
N-BOC-210	13	0.6022	23.6

3.3. Chemical Composition by FT-IR and XPS. The samples were further analyzed by FT-IR, as shown in Figure 5(a). The "free" CO_3^{2-} group (point group symmetry D_{3h}) had four internal vibrations, including 1067 cm^{-1} (symmetric stretching mode ν_1), 846 and 820 cm^{-1} (out of plane bending mode ν_2), 1468 and 1391 cm^{-1} (anti-symmetric vibration ν_3), and 670 cm^{-1} (in-plane deformation ν_4). Besides, vibration peaks of 1756 and 1730 cm^{-1} ($\nu_1 + \nu_4$) are observed for both samples [20]. Figure 5(a) also shows that the peak intensity associated with CO_3^{2-} group increases with HT increasing from 150, 180 to 210°C. The broad peak at 1500–1600 cm^{-1} can be assigned to the characteristic stretching vibrations of hydroxyl groups, derived from the absorbed water molecule [20]. When the ammonia solution was not added during synthesis, the bismuth citrate would not be decomposed and CO_3^{2-} group would not be produced [47]. Hence, a potential conclusion may be postulated that bismuth citrate was first hydrolyzed by the ammonia, followed by decomposition of citrate ions to produce CO_3^{2-} ions during hydrothermal treatment.

The XPS measurements were applied to determine the chemical state of the doped nitrogen, as shown in Figure 5(b). The N1s peak centers at 400.4 eV, which indicates that nitrogen was in situ doped into the $(BiO)_2CO_3$ structure during the hydrothermal reaction. The doped nitrogen atomic ratio of N-BOC-180 samples was measured to be 0.55%. The doped nitrogen must be derived from the ammonia solution added in the precursor solution. The ammonia acts as a dual role in the synthesis of N-doped $(BiO)_2CO_3$. One is to hydrolyze

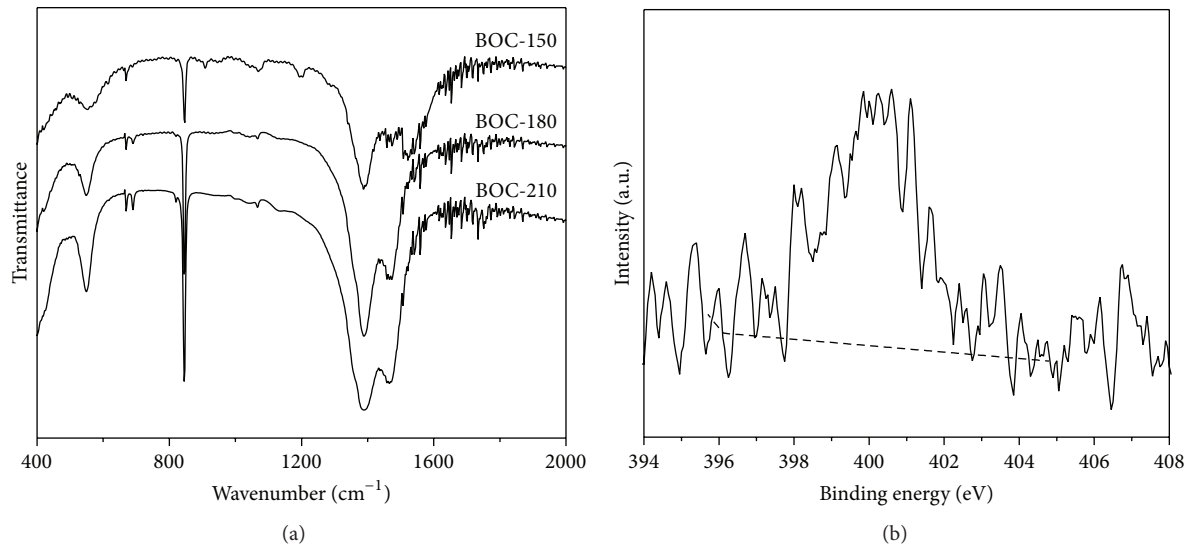

Figure 5: FT-IR spectra of N-BOC-150, N-BOC-180, and N-BOC-210 samples (a) and XPS spectra of N-BOC-180 for N1s (b).

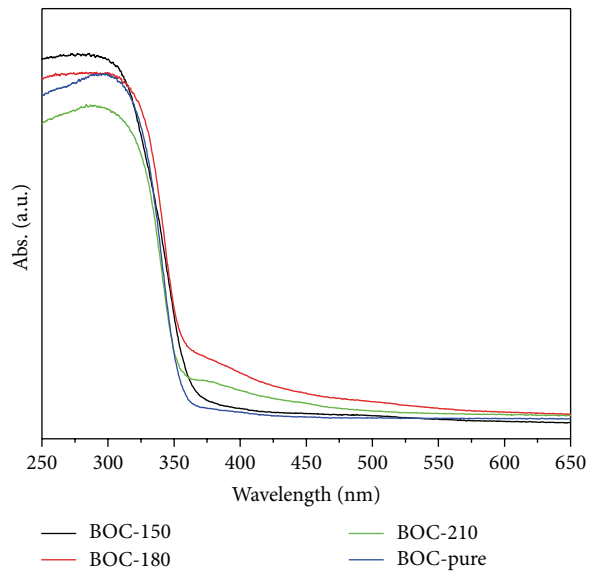

Figure 6: UV-vis DRS of BOC, N-BOC-150, N-BOC-180, and N-BOC-210 samples.

bismuth citrate and the other is to engage in nitrogen doping sources [48]. The N1s peaks approximately at 400.4 eV have been observed in the widely used N-doped TiO_2, where nitrogen substituted for oxygen in TiO_2 and subsequently narrowed the band gap value due to the hybridization of N and O orbital in valence band [48, 49]. Under this mechanism, the doped nitrogen may also substitute for oxygen in $(BiO)_2CO_3$ molecular, which could subsequently modify the band structure and enhance light absorption proficiency of $(BiO)_2CO_3$ (Figure 6). Nevertheless, on account of the presence of two different kinds of oxygen atoms in $(BiO)_2CO_3$ (Bi–O and C–O), current investigations are far from sufficient to reveal which oxygen atom is substituted significantly by the doped nitrogen. Further theoretical investigation about potential mechanisms on this issue is underway.

3.4. UV-Vis DRS Analysis. The UV-vis DRS spectra of N-BOC-150, N-BOC-180, N-BOC-210, and the undoped $(BiO)_2CO_3$ are shown in Figure 6. Utilizing VIL to stimulate photocatalytic reactions is a key challenge since lots of oxide photocatalysts mainly absorb UV light. Compared to undoped $(BiO)_2CO_3$, the three nitrogen-doped $(BiO)_2CO_3$ samples exhibit enhanced visible light absorption. Besides, the absorption edges shift from 330 nm to 350 nm. Furthermore, the as-prepared N-BOC-180 demonstrates the most intensity of VIL absorption, which could be the crucial factor for VIL photocatalytic activities. Combining with the XPS result, the doped nitrogen has made a vital effect on enhancing the VIL absorption. The changes of the absorption spectra were also suggested by the color variation of samples from white for undoped $(BiO)_2CO_3$ to yellow for N-doped $(BiO)_2CO_3$.

Meanwhile, the light absorption in the UV region indicates that the absorption intensity decreases as the HT increases from 150, 180 to 210°C. Compared with N-BOC-210, the enhanced UV absorption of BOC-150 and BOC-180 can be attributed to the self-assembled hierarchical microstructure (Figures 2(a)and 3(c)). As conceivable illustration, the absorbed UV light can be multiply reflected between the interconnected nanosheets, subsequently enhancing the light absorption and utilization [25].

3.5. Photocatalytic Activity under Visible Light Irradiation. The photocatalytic performance of as-prepared N-doped $(BiO)_2CO_3$was further evaluated by removal of NO in a continuous gas phase reactor in order to demonstrate their potential ability for air purification using visible light (Figure 7). There are four reactions related to the photocatalytic reactivity, in which NO reacted with the

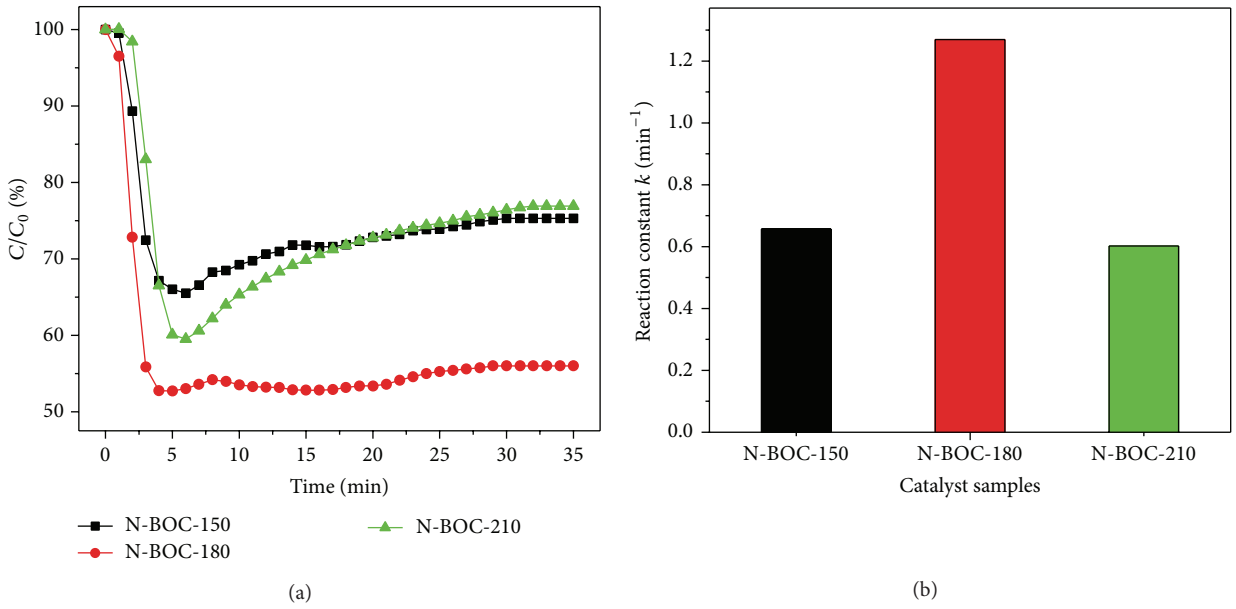

FIGURE 7: Photocatalytic activity of the as-prepared N-BOC-150, N-BOC-180, N-BOC-210 and undoped $(BiO)_2CO_3$ samples for removal of NO under visible light irradiation ($\lambda > 420$ nm) (a), and reaction rate constant at room temperature (b).

photo-generated reactive radicals and produced HNO_2 and HNO_3 displayed in (2)–(5) [50]:

$$NO + 2 \bullet OH \longrightarrow NO_2 + H_2O \quad (2)$$

$$NO_2 + \bullet OH \longrightarrow NO_3^- + H^+ \quad (3)$$

$$NO + NO_2 + H_2O \longrightarrow 2HNO_2 \quad (4)$$

$$NO + \bullet O_2^- \longrightarrow NO_3^- \quad (5)$$

Figure 7(a) shows the variation of NO concentration (C/C_0%) with irradiation time t over the samples under VIL irradiation ($\lambda > 420$ nm). Here, C_0 presents the initial concentration of NO, and C represents the instant concentration of NO during the photocatalytic reaction. NO could not be degraded without photocatalyst or without light irradiation. Under the irradiation of visible light and presence of photocatalyst, the as-prepared photocatalytic materials, NO reacts with the photo-generated reactive radicals to produce final NO_3^- product [51]. The undoped $(BiO)_2CO_3$ showed negligible VIL activity due to its UV absorption [44]. As shown in Figure 7(a), NO concentration decreases rapidly for all N-doped $(BiO)_2CO_3$ in the first 5 min. The initial reaction rate constants of N-BOC-150, N-BOC-180, and N-BOC-210 were 0.6570, 1.2698, and 0.6022 min^{-1} (Table 2, Figure 7(b)), which were much higher than those of undoped $(BiO)_2CO_3$ [44]. The improved visible light photocatalytic activity may be ascribed to the nitrogen doping (Figures 2, 3, and 4) and hierarchical structures (Figures 2 and 3) compared with that of pure BOC [43, 44].

However, after about 6 min, the removal ratio of NO decreases slightly, which should be ascribed to the intermediates and final products, occupying the active sites of photocatalyst. After about 35 min irradiation, the removal rates of N-BOC-180 (44.1%) are higher than those of N-BOC-150 (24.7%) and N-BOC-210 (23.6%) (Table 2). Besides, the NO removal ratio reaches about 20.3% over C-doped TiO_2, which is well known as a good VIL-driven photocatalyst [22]. Also, the N-doped TiO_2 demonstrated good VIL activities, by which the NO removal rates could reach to about 36% from well published articles [52]. Inspiringly, the as-prepared N-BOC-180 hierarchical microspheres exhibit superior photocatalytic activity with NO removal rates highly reaching up to 44.1% under VIL irradiation, much higher than that of C-doped TiO_2 and N-doped TiO_2.

Nevertheless, the S_{BET} of N-BOC-180 is much lower than that of C-doped TiO_2 (122.5 m^2/g) (Table 2) [20], from which we can draw a conclusion that S_{BET} could not be the dominant factor for the outstanding photocatalytic activity of N-BOC-180. Furthermore, recent reports have demonstrated that the hierarchical and hollow structures have significant advantages in enhancing the photocatalytic activity. A novel0020$BiVO_4/Bi_2O_2CO_3$ hierarchical micro/nanoarchitecture prepared by Madhusudan et al. exhibited wonderful photocatalytic performance due to the inhibition of electron/hole pair recombination [26]. The hollow NiO microspheres fabricated by Song and Gao have showed notably enhanced photocatalytic activity over NiO rods due to the increasing number of surface active sites and enhanced surface charge carrier transfer rate [53]. Thus, the conspicuously outstanding VIL photocatalytic activity of N-BOC-180 could mainly be ascribed to the special hierarchical and hollow structure. With nanoplates self-assembled hierarchical structure, multiple light reflections were extraordinarily strengthened between the interconnected nanosheets, thus enhancing light-harvesting and increasing the quantity of photogenerated electrons and holes available to participate in the photocatalytic redox reaction. Furthermore,

the extremely decent activity of N-BOC-180 samples is much higher than that of N-BOC-150. This result can be ascribed to the following potential factors. The larger surface areas (Table 1) and more smooth nanosheets (Figures 2(b) and 3(b)) can both successfully accelerate immediate transfer for intermediates and final products; in spite of that both of them have the same hierarchical morphology with a hollow in the center. Therefore, the remarkable photocatalytic activity may be dominated mainly by the synergy effects of the two factors mentioned above. The present work not only gains deeper understanding of temperature-dependent morphology-controlling mechanisms for N-BOC fabrication, but also paves the way for further modification of $(BiO)_2CO_3$ with higher performance for environmental pollution control.

4. Conclusion

In summary, we have developed a one-pot template-free method to synthesize N-doped $(BiO)_2CO_3$ hierarchical microspheres based on hydrothermal treatment of bismuth citrate and concentrated ammonia solution in water. N-BOC with different morphologies (rosa chinensis-like, red camellia-like and lamina-like nanostructures) was fabricated based on different HT ranging from 150, 180 to 210°C. The rosa chinensis-like N-BOC-150 and red camellia-like, N-BOC-180 was hierarchically self-assembled by nanosheets, while the lamina-like N-BOC-210 was randomly composed of abundant irregular nanosheets. The thickness of nanoplates was augmented with the increasing HT. Moreover, the as-prepared N-BOC-180 exhibited the highest photocatalytic activity, which was ascribed to the special hierarchical morphology and the enhanced visible light absorption. This work not only elucidates the mechanism of temperature-dependent morphology control on $(BiO)_2CO_3$ fabrication, but also opens new avenue for the design of optimized photocatalysts with enhanced visible-light-driven activity.

Conflict of Interests

The authors declare that they do not have any conflict of interests.

Acknowledgments

This research is financially supported by the Science and Technology Project of CQ CSTC (stc2013yykfB50008, cstc2013jcyjA20018), the Science and Technology Project from Chongqing Education Commission (KJ120713, KJ130725), the Innovative Research Team Development Program in University of Chongqing (KJTD201314), and the key discipline development project of CTBU (1252001).

References

[1] M. R. Hoffmann, S. T. Martin, W. Choi, and D. W. Bahnemann, "Environmental applications of semiconductor photocatalysis," *Chemical Reviews*, vol. 95, no. 1, pp. 69–96, 1995.

[2] Y. Li, X. Fang, N. Koshizaki et al., "Periodic TiO_2 nanorod arrays with hexagonal nonclose-packed arrangements: excellent field emitters by parameter optimization," *Advanced Functional Materials*, vol. 19, no. 15, pp. 2467–2473, 2009.

[3] Y. Li, T. Sasaki, Y. Shimizu, and N. Koshizaki, "A hierarchically ordered TiO_2 hemispherical particle array with hexagonal-non-close-packed tops: synthesis and stable superhydrophilicity without UV irradiation," *Small*, vol. 4, no. 12, pp. 2286–2291, 2008.

[4] F. Dong, H. Q. Wang, S. Guo, Z. B. Wu, and S. C. Lee, "Enhanced visible light photocatalytic activity of novel Pt/C-doped $TiO_2/PtCl_4$ three-component nanojunction system for degradation of toluene in air," *Journal of Hazardous Materials*, vol. 187, no. 1–3, pp. 509–516, 2011.

[5] F. Dong, Y. J. Sun, and M. Fu, "Enhanced visible light photocatalytic activity of V_2O_5 cluster modified N-doped TiO_2 for degradation of toluene in air," *International Journal of Photoenergy*, vol. 2012, Article ID 569716, 10 pages, 2012.

[6] F. Dong, S. Guo, H. Q. Wang, X. F. Li, and Z. B. Wu, "Enhancement of the visible light photocatalytic activity of C-doped TiO_2 nanomaterials prepared by a green synthetic approach," *The Journal of Physical Chemistry C*, vol. 115, no. 27, pp. 13285–13292, 2011.

[7] Z. F. Bian, J. Zhu, S. H. Wang, Y. Cao, X. F. Qian, and H. X. Li, "Self-assembly of active Bi_2O_3/TiO_2 visible photocatalyst with ordered mesoporous structure and highly crystallized anatase," *The Journal of Physical Chemistry C*, vol. 112, no. 16, pp. 6258–6262, 2008.

[8] J. Tang, Z. Zou, and J. H. Ye, "Efficient photocatalytic decomposition of organic contaminants over $CaBi_2O_4$ under visible-light irradiation," *Angewandte Chemie—International Edition*, vol. 43, no. 34, pp. 4463–4466, 2004.

[9] Z. Zhu, L. Zhang, J. Li, J. Du, Y. Zhang, and J. Zhou, "Synthesis and photocatalytic behavior of $BiVO_4$ with decahedral structure," *Ceramics International*, vol. 39, no. 7, pp. 7461–7465, 2013.

[10] Z. Chen, L. W. Qian, J. Zhu, Y. P. Yuan, and X. F. Qian, "Controlled synthesis of hierarchical Bi_2WO_6 microspheres with improved visible-light-driven photocatalytic activity," *CrystEngComm*, vol. 12, no. 7, pp. 2100–2106, 2010.

[11] Y. Q. Lei, G. H. Wang, S. Y. Song et al., "Room temperature, template-free synthesis of BiOI hierarchical structures: visible-light photocatalytic and electrochemical hydrogen storage properties," *Dalton Transactions*, vol. 39, no. 13, pp. 3273–3278, 2010.

[12] X. Zhang, Z. H. Ai, F. L. Jia, and L. Z. Zhang, "BiOCl nano/microstructures on substrates: synthesis and photocatalytic properties," *The Journal of Physical Chemistry C*, vol. 112, no. 7, pp. 747–753, 2008.

[13] T. Wu, X. G. Zhou, H. Zhang, and X. H. Zhong, "Bi_2S_3 nanostructures: a new photocatalyst," *Nano Research*, vol. 3, no. 5, pp. 379–386, 2010.

[14] J. D. Grice, "A solution to the crystal structures of bismutite and beyerite," *Canadian Mineralogist*, vol. 40, no. 2, pp. 693–698, 2002.

[15] Y. Zheng, F. Duan, M. Chen, and Y. Xie, "Synthetic $Bi_2O_2CO_3$ nanostructures: novel photocatalyst with controlled special surface exposed," *Journal of Molecular Catalysis A*, vol. 317, no. 1-2, pp. 34–40, 2010.

[16] Y. Y. Liu, Z. Y. Wang, B. B. Huang et al., "Preparation, electronic structure, and photocatalytic properties of $Bi_2O_2CO_3$ nanosheet," *Applied Surface Science*, vol. 257, no. 1, pp. 172–175, 2010.

[17] R. Chen, G. Cheng, M. H. So et al., "Bismuth subcarbonate nanoparticles fabricated by water-in-oil microemulsion-assisted hydrothermal process exhibit anti-Helicobacter pylori properties," *Materials Research Bulletin*, vol. 45, no. 5, pp. 654–658, 2010.

[18] Y. Zhou, H. Wang, M. Sheng et al., "Environmentally friendly room temperature synthesis and humidity sensing applications of nanostructured $Bi_2O_2CO_3$," *Sensors and Actuators B*, vol. 188, no. 2013, pp. 1312–1318, 2013.

[19] T. Zhao, J. T. Zai, M. Xu et al., "Hierarchical $Bi_2O_2CO_3$ microspheres with improved visible-light-driven photocatalytic activity," *CrystEngComm*, vol. 13, no. 12, pp. 4010–4017, 2011.

[20] F. Dong, S. C. Lee, Z. Wu et al., "Rose-like monodisperse bismuth subcarbonate hierarchical hollow microspheres: one-pot template-free fabrication and excellent visible light photocatalytic activity and photochemical stability for NO removal in indoor air," *Journal of Hazardous Materials*, vol. 195, pp. 346–354, 2011.

[21] P. Madhusudan, J. Zhang, B. Cheng, and G. Liu, "Photocatalytic degradation of organic dyes with hierarchical $Bi_2O_2CO_3$ microstructures under visible light," *CrystEngComm*, vol. 15, no. 2, pp. 231–240, 2013.

[22] F. Dong, W.-K. Ho, S. C. Lee et al., "Template-free fabrication and growth mechanism of uniform $(BiO_2)CO_3$ hierarchical hollow microspheres with outstanding photocatalytic activities under both UV and visible light irradiation," *Journal of Materials Chemistry*, vol. 21, no. 33, pp. 12428–12436, 2011.

[23] H. C. Zeng, "Ostwald ripening: a synthetic approach for hollow nanomaterials," *Current Nanoscience*, vol. 3, no. 2, pp. 177–181, 2007.

[24] H. J. Fan, U. Gösele, and M. Zacharias, "Formation of nanotubes and hollow nanoparticles based on kirkendall and diffusion processes: a review," *Small*, vol. 3, no. 10, pp. 1660–1671, 2007.

[25] J. Zhang, F. Huang, and Z. Lin, "Progress of nanocrystalline growth kinetics based on oriented attachment," *Nanoscale*, vol. 2, no. 1, pp. 18–34, 2010.

[26] P. Madhusudan, J. Ran, J. Zhang, J. Yu, and G. Liu, "Novel urea assisted hydrothermal synthesis of hierarchical $BiVO_4$/$Bi_2O_2CO_3$ nanocomposites with enhanced visible-light photocatalytic activity," *Applied Catalysis B*, vol. 110, pp. 286–295, 2011.

[27] M. Yang, J. Ma, C. L. Zhang, Z. Z. Yang, and Y. F. Lu, "General synthetic route toward functional hollow spheres with double-shelled structures," *Angewandte Chemie—International Edition*, vol. 117, no. 41, pp. 6885–6888, 2005.

[28] J. G. Yu and X. X. Yu, "Hydrothermal synthesis and photocatalytic activity of zinc oxide hollow spheres," *Environmental Science and Technology*, vol. 42, no. 13, pp. 4902–4907, 2008.

[29] S.-W. Kim, M. Kim, W. Y. Lee, and T. Hyeon, "Fabrication of hollow palladium spheres and their successful application to the recyclable heterogeneous catalyst for suzuki coupling reactions," *Journal of the American Chemical Society*, vol. 124, no. 26, pp. 7642–7643, 2002.

[30] J. H. Gao, B. Zhang, X. X. Zhang, and B. Xu, "Magnetic-dipolar-interaction-induced self-assembly affords wires of hollow nanocrystals of cobalt selenide," *Angewandte Chemie—International Edition*, vol. 45, no. 8, pp. 1220–1223, 2006.

[31] A. D. Dinsmore, M. F. Hsu, M. G. Nikolaides, M. Marquez, A. R. Bausch, and D. A. Weitz, "Colloidosomes: selectively permeable capsules composed of colloidal particles," *Science*, vol. 298, no. 5595, pp. 1006–1009, 2002.

[32] Y. S. Li, J. L. Shi, Z. L. Hua, H. R. Chen, M. L. Ruan, and D. S. Yan, "Hollow spheres of mesoporous aluminosilicate with a three-dimensional pore network and extraordinarily high hydrothermal stability," *Nano Letters*, vol. 3, no. 5, pp. 609–612, 2003.

[33] H. G. Yang and H. C. Zeng, "Creation of intestine-like interior space for metal-oxide nanostructures with a quasi-reverse emulsion," *Angewandte Chemie—International Edition*, vol. 43, no. 39, pp. 5206–5209, 2004.

[34] D. H. M. Buchold and C. Feldmann, "Nanoscale γ-AlO(OH) hollow spheres: synthesis and container-type functionality," *Nano Letters*, vol. 7, no. 11, pp. 3489–3492, 2007.

[35] J. Zhou, W. Wu, D. Caruntu et al., "Synthesis of porous magnetic hollow silica nanospheres for nanomedicine application," *The Journal of Physical Chemistry C*, vol. 111, no. 47, pp. 17473–17477, 2007.

[36] M. R. Jones, K. D. Osberg, R. J. MacFarlane, M. R. Langille, and C. A. Mirkin, "Templated techniques for the synthesis and assembly of plasmonic nanostructures," *Chemical Reviews*, vol. 111, no. 6, pp. 3736–3827, 2011.

[37] J. G. Yu and X. X. Yu, "Hydrothermal synthesis and photocatalytic activity of zinc oxide hollow spheres," *Environmental Science and Technology*, vol. 42, no. 13, pp. 4902–4907, 2008.

[38] R. Asahi, T. Morikawa, T. Ohwaki, K. Aoki, and Y. Taga, "Visible-light photocatalysis in nitrogen-doped titanium oxides," *Science*, vol. 293, no. 5528, pp. 269–271, 2001.

[39] A. Fujishima, X. T. Zhang, and D. A. Tryk, "TiO_2 photocatalysis and related surface phenomena," *Surface Science Reports*, vol. 63, no. 12, pp. 515–582, 2008.

[40] J. Hou, R. Cao, Z. Wang, S. Jiao, and H. Zhu, "Hierarchical nitrogen doped bismuth niobate architectures: controllable synthesis and excellent photocatalytic activity," *Journal of Hazardous Materials*, vol. 217-218, pp. 177–186, 2012.

[41] F. Zou, Z. Jiang, X. Qin et al., "Template-free synthesis of mesoporous N-doped $SrTiO_3$ perovskite with high visiblelight-driven photocatalytic activity," *Chemical Communications*, vol. 48, no. 68, pp. 8514–8516, 2012.

[42] A. Mukherji, B. Seger, G. Q. Lu, and L. Wang, "Nitrogen doped $Sr_2Ta_2O_7$ coupled with graphene sheets as photocatalysts for increased photocatalytic hydrogen production," *ACS Nano*, vol. 5, no. 5, pp. 3483–3492, 2011.

[43] F. Dong, Y. J. Sun, W. K. Ho, and Z. B. Wu, "Controlled synthesis, growth mechanism and highly efficient solar photocatalysis of nitrogen-doped bismuth subcarbonate hierarchical nanosheets architectures," *Dalton Transactions*, vol. 41, no. 27, pp. 8270–8284, 2012.

[44] F. Dong, T. Xiong, Z. W. Zhao, Y. J. Sun, and M. Fu, "Ammonia induced formation of N-doped $(BiO_2)CO_3$ hierarchical microspheres: the effect of hydrothermal temperature on the morphology and photocatalytic activity," *CrystEngComm*, vol. 15, no. 48, pp. 10522–10532, 2013.

[45] Z. H. Ai, L. L. Zhu, S. C. Lee, and L. Z. Zhang, "NO treated TiO_2 as an efficient visible light photocatalyst for NO removal," *Journal of Hazardous Materials*, vol. 192, no. 1, pp. 361–367, 2011.

[46] F. Dong, H. Q. Wang, and Z. B. Wu, "One-step "green" synthetic approach for mesoporous C-doped TiO_2 with efficient visible light photocatalytic activity," *The Journal of Physical Chemistry C*, vol. 113, no. 38, pp. 16717–16723, 2009.

[47] F. Dong, A. M. Zheng, Y. J. Sun et al., "One-pot template-free synthesis, growth mechanism and enhanced photocatalytic activity of monodisperse $(BiO_2)CO_3$ hierarchical hollow microspheres self-assembled with single-crystalline nanosheets," *CrystEngComm*, vol. 14, no. 10, pp. 3534–3544, 2012.

[48] X. B. Chen and C. Burda, "Photoelectron spectroscopic investigation of nitrogen-doped titania nanoparticles," *The Journal of Physical Chemistry B*, vol. 108, no. 40, pp. 15446–15449, 2004.

[49] Q. J. Xiang, J. G. Yu, W. G. Wang, and M. Jaroniec, "Nitrogen self-doped nanosized TiO_2 sheets with exposed 001 facets for enhanced visible-light photocatalytic activity," *Chemical Communications*, vol. 47, no. 24, pp. 6906–6908, 2011.

[50] H. T. Tian, J. W. Li, M. Ge, Y. P. Zhao, and L. Liu, "Removal of bisphenol A by mesoporous BiOBr under simulated solar light irradiation," *Catalysis Science & Technology*, vol. 2, no. 11, pp. 2351–2355, 2012.

[51] F. Dong, H. T. Liu, W. K. Ho, M. Fu, and Z. B. Wu, "$(NH_4)_2CO_3$ mediated hydrothermal synthesis of N-doped $(BiO_2)CO_3$ hollow nanoplates microspheres as high-performance and durable visible light photocatalyst for air cleaning," *Chemical Engineering Journal*, vol. 214, no. 10, pp. 198–207, 2013.

[52] Z. H. Ai, W. K. Ho, S. C. Lee, and L. Z. Zhang, "Efficient photocatalytic removal of NO in indoor air with hierarchical bismuth oxybromide nanoplate microspheres under visible light," *Environmental Science and Technology*, vol. 43, no. 11, pp. 4143–4150, 2009.

[53] X. F. Song and L. Gao, "Facile synthesis and hierarchical assembly of hollow nickel oxide architectures bearing enhanced photocatalytic properties," *The Journal of Physical Chemistry C*, vol. 112, no. 39, pp. 15299–15305, 2008.